Mesoporous Silica Hollow Spheres with Ordered Radial Mesochannels by a Spontaneous Self-Transformation Approach

ARTICLE *in* CHEMISTRY OF MATERIALS · DECEMBER 2012

Impact Factor: 8.35 · DOI: 10.1021/cm303338v

10 AUTHORS, INCLUDING:

Zhaogang Teng
Nanjing University
27 PUBLICATIONS **300** CITATIONS
SEE PROFILE

Jing Sun
Hamilton Family Health Team
273 PUBLICATIONS **3,369** CITATIONS
SEE PROFILE

Chen Guotao
Nanjing University
6 PUBLICATIONS **81** CITATIONS
SEE PROFILE

CHEMISTRY OF MATERIALS

Article

pubs.acs.org/cm

Mesoporous Silica Hollow Spheres with Ordered Radial Mesochannels by a Spontaneous Self-Transformation Approach

Zhaogang Teng,[†] Xiaodan Su,[‡] Yuanyi Zheng,[∥] Jing Sun,[†] Guotao Chen,[†] Congcong Tian,[†] Jiandong Wang,[†] Hao Li,[†] Yane Zhao,[†] and Guangming Lu*[,†]

[†]Department of Medical Imaging, Jinling Hospital, Clinical School of Medical College, Nanjing University, Nanjing 210002, P.R. China

[‡]Key Laboratory for Organic Electronics & Information Displays and Institute of Advanced Materials, Nanjing University of Posts and Telecommunications, Nanjing 210046, P.R. China

[∥]Second Affiliated Hospital of Chongqing Medical University, Chongqing 400010, P.R. China

Supporting Information

ABSTRACT: We demonstrate a self-transformation approach for the synthesis of ordered mesoporous silica hollow spheres with radially oriented mesochannels. The method is simple and facile, in which mesostructured silica spheres synthesized in a Stöber solution can spontaneously transform to hollow structure when they are incubated with water. The formation of the hollow structure does not require any sacrificial templates, emulsion droplets, or surface protective agents. The obtained mesoporous silica hollow spheres possess controllable diameter, tunable shell thickness, high specific surface area, and uniform mesopore. Transmission electron microscopy (TEM) observations show that the formation of the hollow spheres undergoes a selective etching process in the inner section. ^{29}Si NMR spectra and detailed reactions demonstrate that the solid-to-hollow transformation of the Stöber silica spheres in water is attributed to the difference in the degree of condensation of silica between their outer layer and inner section. Cytotoxicity and histological assays confirm that the obtained mesoporous silica hollow spheres possess good biocompatibility. Besides, the capability of the hollow spheres as contrast agents for untrasound imaging is conducted in vitro. Moreover, yolk–shell microspheres with a Fe_3O_4@ $nSiO_2$ core and a mesoporous silica shell are successfully prepared based on the facile self-transformation strategy, which provides a general method to create various yolk–shell structured multifunctional composites for different applications.

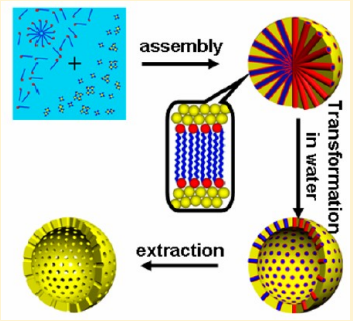

KEYWORDS: *hollow spheres, mesoporous, silica, self-transformation, yolk–shell*

1. INTRODUCTION

Hollow and yolk–shell structured mesoporous silica has attracted increasing attention in recent years and has been applied in many important research fields,[1−12] such as catalysis,[4,5] drug/gene delivery,[6−9] and medical imaging,[10−12] owing to its properties of uniform pore size, high surface area, large void space, abundant Si–OH active bonds, and good biocompatibility. Previously, mesoporous hollow spheres have been synthesized by self-assembly of silica precursors with surfactant templates at oil–water[1,2,13,14] or air–water droplet interfaces,[15] or using the vesicle approach.[3,16,17] As these soft templates generally represent low stability and poor uniformity in solution, the obtained hollow materials are often ill-defined in shape and polydispersed in size. Also, the hollow core size and shell thickness cannot be easily and independently controlled by these techniques. To overcome these problems, the hard templating methods have been used to fabricate mesoporous silica hollow spheres by using polymer[5,18−20] or inorganic beads[6,21−23] as sacrificial core templates. However, the preparation and removal procedures of the sacrifical templates are generally complicated, uneconomic, and time-consuming. Therefore, it is highly valuable to develop a facile and effective strategy for preparing the hierarchical structures.

The Stöber approach is a well-known and efficacious process to synthesize uniform spherical colloid silica particles via the hydrolysis and condensation of tetraethoxysilane (TEOS) in ethanol aqueous solution.[24] The Stöber method derived uniform silica spheres brought great opportunities for facile preparation of hollow silica structure through template-free methods. It was reported that hollow silica spheres can be prepared through selectively etching the inner section of colloid silica particles by using polymers to protect the outmost layer.[25−27] Silica spheres with hollow or yolk–shell structures also have been fabricated by one-pot sequential condensation of 3-aminopropyltriethoxysilane (APTES) and TEOS and then etching the less compact internal organic-silica layers with HF or ammonia.[28,29] Recently, Chen and co-workers found that the outer layer of the nonporous silica particles formed by the Stöber method is chemically more robust than the inner layer,

Received: October 16, 2012
Revised: December 10, 2012
Published: December 14, 2012

which can be selectively etched to form hollow and yolk−shell particles.[30] However, these self-templating methods often require using surface protective polymers or extremely corrosive etching agents, and the silica shells derived from nonporous colloid silica particles do not possess accessible ordered mesopores.[25−32] The etching agents are hard completely wash away, and they are harmful for the body. The silica shells make it difficult for outside molecules to be loaded in the hollow spheres. As a result, these hollow silica particles are limited in the applications, particularly, in biosystems and biomedicine. We recently found that the Stöber method can be utilized to synthesize ordered mesoporous silica films with perpendicular mesochannels by a self-assembly process in the presence of surfactant templates.[33] Furthermore, a new type of sandwich-like mesoporous silica films with hollow structures inside can also be obtained by increasing the silica solubility in solution. This exciting result inspires us to develop a facile approach for fabricating mesoporous silica hollow particles.

Herein, we present that Stöber method derived silica spheres with radially oriented mesostructure undergo a spontaneous morphology change from solid to hollow when they are incubated in water. The spontaneous transformation process is very simple, effective, scalable, eco-friendly, and even low cost, which represents a unique methodological advantage for tuning the structure of mesoporous silica. The structures and transformation process of the mesoporous silica hollow spheres were investigated by scanning electron microscopy (SEM), small-angle X-ray diffraction (XRD), and transmission electron microscopy (TEM). The obtained hollow spheres possess controllable size, tunable shell thickness, high surface area, and radially oriented ordered mesochannels. Moreover, we also demonstrate that the facile spontaneous self-transformation strategy can be used to prepare yolk−shell structures with functional interior core and radially oriented mesoporous shell. Biocompatibility of the hollow spheres based on cytotoxicity and histopathological examinations permits its future biomedicine applications. As a proof-of-concept for their application, the hollow silica spheres show a potential for ultrasound imaging.

2. EXPERIMENTAL SECTION

2.1. Materials. Analytical reagents of anhydrous ethanol, concentrated ammonia aqueous solution (25 wt %), TEOS, and cetyltrimethylammonium bromide (CTAB) were purchased from Sinopharm Chemical Reagent Co., Ltd. Deionized water (Millipore) with a resistivity of 18 MΩ cm was used in all experiments. RPMI 1640 medium, heat-inactivated fetal bovine serum (FBS), and penicillin−streptomycin solution were purchased from Gibco Laboratories (Invitrogen Co, Grand Island, NY, U.S.A.). Cell counting kit-8 (CCK-8) was purchased from Nanjing Keygen Biotech. Co., Ltd. (Nanjing, China). The human embryo kidney 293T cell line was obtained from American Type Culture Collection (ATCC).

2.2. Synthesis of Mesoporous Silica Hollow Spheres. Mesostructured silica spheres were prepared via a surfactant-assembly sol−gel process in a Stöber solution containing CTAB, TEOS, ammonia, and ethanol. Typically, CTAB was dissolved in ethanol aqueous solution containing concentrated ammonia aqueous solution (1 mL, 25 wt %). Then, the mixture was heated to 35 °C, and TEOS (1 mL) was rapidly added under vigorous stirring. The molar ratio of the reaction mixture was 1.00 TEOS:0.0922 CTAB:2.96 NH_3:621 H_2O:115 C_2H_5OH. After stirring at 35 °C for 24 h, the white product was collected by centrifugation at 4000 rpm for 10 min and washed three times with ethanol. Then, the Stöber method derived silica product was dispersed in water to prepare the mesoporous silica hollow spheres via the spontaneous self-transformation approach. Briefly, the as-made Stöber silica spheres were incubated in pure water (160 mL) at 25−90 °C for 2−148 h and then collected by centrifugation and washed three times with ethanol. To remove the pore-generating template (CTAB), the as-synthesized materials were transferred to an ethanol solution (120 mL) containing concentrated HCl (240 μL, 37%) and stirred at 60 °C for 3 h. The surfactant extraction step was repeated two times to ensure complete removal of CTAB. The template-removed mesoporous silica hollow spheres were washed with ethanol three times and dried under high vacuum. The mesoporous silica hollow spheres with small sizes and thin shell thicknesses were obtained by adjusting the ethanol/water ratio of the Stöber solution and then incubated in 400 mL of water at 70 °C for 12 h.

2.3. Synthesis of Yolk−Shell Structured Magnetic Mesoporous Microspheres. The spherical magnetite particles with a mean diameter of about 300 nm were prepared according to preciously reported solvothermal reaction.[34] Briefly, $FeCl_3$ (0.65 g), trisodium citrate dehydrate (0.20 g), and sodium acetate (1.20 g) were dissolved in ethylene glycol (20 mL) under magnetic stirring. The obtained homogeneous yellow solution was transferred to a Teflon-lined stainless-steel autoclave with a capacity of 30 mL. The autoclave was heated to 200 °C and maintained for 10 h, and then, it was cooled down to room temperature. The obtained black magnetite particles were washed with water for five times and then dried in vacuum at 60 °C for 12 h. The obtained Fe_3O_4 particles were used to prepare core−shell Fe_3O_4@$nSiO_2$ spheres through a versatile Stöber sol−gel method.[35,36] Typically, the Fe_3O_4 particles (0.08 g) were homogeneously dispersed in an ethanol aqueous solution containing concentrated ammonia aqueous solution (1.7 mL, 25 wt %), followed by the addition of TEOS (140 μL). The mass ratio of the reaction mixture in grams was 1.00 TEOS:2.94 NH_3:7.68 H_2O:303 C_2H_5OH:0.614 Fe_3O_4. After stirring at 40 °C for 6 h, the Fe_3O_4@$nSiO_2$ spheres were obtained and washed five times with water. The above prepared Fe_3O_4@$nSiO_2$ spheres (0.016 g) were dispersed in an ethanol aqueous solution containing concentrated ammonia aqueous solution (25 wt %) and CTAB. Then, TEOS (1 mL) was added to the dispersion under stirring. The stirring speed of the reaction solution was controlled at 300 rpm by using a D2004 electric stirrer (Shanghai Meiyingpu Co., Ltd.). The mass ratio of the reaction mixture in grams was 1.00 TEOS:0.161 CTAB:0.242 NH_3:53.8 H_2O:25.5 C_2H_5OH:0.0172 Fe_3O_4@$nSiO_2$. After reaction at 35 °C for 24 h, the products were collected with a magnet and washed with water and ethanol five times. Afterward, the products were incubated in water (160 mL) at 70 °C for 12 h. To remove the pore-generating template (CTAB), the as-synthesized materials were transferred to ethanol (120 mL) with continual stirring at 60 °C for 3 h. The surfactant extraction step was repeated twice to ensure removal of CTAB. The template-removed magnetic mesoporous silica microspheres were washed with ethanol twice and dried under high vacuum.

2.4. Cell Culture and Viability Assay. Cells were routinely grown in 75 cm^2 plastic culture flasks in RPMI 1640 medium supplemented with 10% (v/v) FBS and 1% (v/v) penicillin-streptomycin solution at 37 °C under a 5% CO_2 atmosphere with 95% relative humidity. For the cytotoxicity assay of mesoporous silica hollow spheres, the cell viability test was performed using cell counting kit-8 (CCK-8). Briefly, cells growing in log phase were seeded into 96-well cell-culture plate at a density of 1×10^4 cells/well. Five duplicate wells were set up for each group. Twenty four hours later, RPMI 1640 medium containing different concentrations of mesoporous silica hollow spheres was added to the cell culture. The cells were grown for an additional 24 h at 37 °C prior to adding CCK-8 solution (10 μL) to the culture. After 5 h incubation at 37 °C, the absorbance (A) was measured using an automated microplate reader (BioTek) at the wavelength of 450 nm. The viability of cell growth was calculated by using the following formula: viability (%) = (mean of absorbance value of treatment group/mean absorbance value of control) × 100. The results were expressed as an average over three nominally identical measurement.

dx.doi.org/10.1021/cm303338v | Chem. Mater. 2013, 25, 98−105

2.5. In Vivo Toxicity Studies. All animal experiments were in agreement with the guidelines of the Institutional Animal Care and Use Committee. Mesoporous silica hollow spheres were injected into 4-week-old male, 20 g ICR mice (n = 3) at a dose of 25 mg kg^{-1} via the tail vein. To examine in vivo toxicity, the liver, spleen, heart, lung, intestine, and kidney were removed at 4 days postinjection and fixed in 10% formalin solution. Then, the tissues were embedded in paraffin, sectioned, and stained with hematoxylin and eosin. The histological sections were observed under an optical microscope (IX71; Olympus, Tokyo, Japan). All the identity and analysis of the pathology slides were blind to the pathologist.

2.6. In Vitro Ultrasound Imaging. The dried mesoporous silica hollow spheres were weighed into 2 mL tubing vials, evacuated, and sparged with perfluoropentane gas at room temperature and sealed for storage. A preliminary evaluation of the ultrasound contrast behavior of the gas encapsulated hollow spheres was carried out using a gel model with 6 coels. Different concentrations of silica spheres dispersed in phosphate-buffered saline (PBS) solution were used to achieve the ultrasound imaging. All the samples were scanned by an ultrasonic diagnostic instrument (12 L; IU22; Philips Medical Systems, Bothell, WA) in conventional B mode and harmonic mode. For comparison, the ultrasound imaging of the solid-core structured mesoporous silica spheres prepared in the same Stöber solution was also measured.

2.7. Characterization. SEM images were obtained on a Hitachi S4800 SEM (Japan) operated at 1 kV and 10 μA. TEM images were taken on a JEOL JEM-2100 microscope (Japan) at 200 kV. The samples were dispersed by ultrasonic in ethanol and dropped on a carbon-coated copper grid for TEM observation. Nitrogen sorption isotherms were measured using a Micromeritics Tristar 3000 analyzer at −196 °C. The samples were degassed at 180 °C for 6 h before the measurements. The Brunauer−Emmett−Teller (BET) method was utilized to calculate the specific surface area (S_{BET}) using the adsorption data at p/p_0 = 0.05−0.15. Pore size analysis was performed by applying proper nonlocal density functional theory (NLDFT) methods from the adsorption branch of the isotherm. The pore wall thickness was evaluated as the difference between the unit cell parameter ($a = 2d_{10}/\sqrt{3}$) and the pore size. The total pore volume (V_{total}) was estimated from the adsorbed amount at p/p_0 = 0.995. The XRD pattern was obtained with a Bruker model D8 focus diffractometer equipped with a copper anode producing X-ray with wavelength of 0.154 nm (40 kV, 40 mA). Data were collected in continuous scan mode from 1 to 10° with a 0.02° sampling interval. The d-spacing value was calculated using the formula $d = 2\pi/q$, where $q = 4\pi(\sin\theta)/\lambda$. A Quantum Design MPMS-XL SQUID magnetometer was used to determine the magnetic characteristics of the magnetic samples. Magnetization curves as a function of magnetic field were measured at 298 K under magnetic fields up to 20 kOe. ^{29}Si magic-angle spinning (MAS) NMR spectra were recorded at 9.47 T on a Bruker AVIII400 spectrometer operating at 79.48 MHz using a 7 mm MAS probe. The measurements were performed with a spin rate of 6.0 kHz and a recycle delay of 80−150 s. The chemical shifts were referenced to 3-(trimethylsilyl)-1-propanesulfonic acid sodium salt (DSS). To evaluate the contents of dissociative silica species in water, the supernatant of the solution was isolated by centrifugation at different time and determined by inductively coupled plasma-atomic emission spectroscopy (ICP-AES) using a Perkin-Elmer Optima-5300DV spectrometer.

3. RESULTS AND DISCUSSION

The synthesis procedure is shown in Figure 1a. First, uniform mesostructured silica spheres were prepared via a surfactant-assembly sol−gel process in a Stöber solution containing CTAB, TEOS, ammonia, and ethanol. Second, the Stöber-solution derived silica spheres spontaneously transformed into hollow spheres when they were incubated with water. Third, CTAB templates were removed by acidic ethanol extraction to form mesoporous shell, resulting in mesoporous silica hollow spheres. TEM images show that the silica spheres prepared via

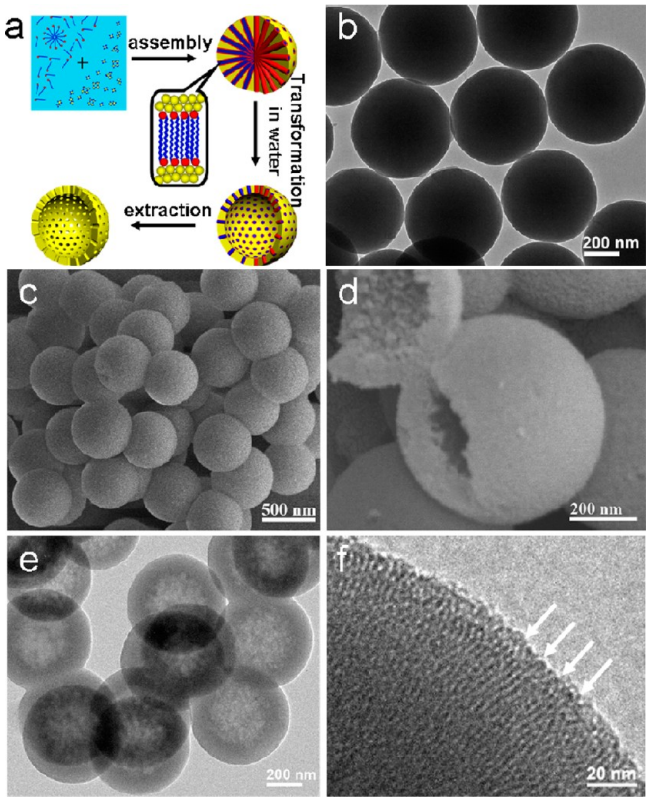

Figure 1. (a) Schematic illustration of preparation process of the mesoporous silica hollow spheres via the spontaneous self-transformation method. (b) TEM image of as-made mesostructured silica spheres. (c) SEM image of hollow silica spheres at low magnification. (d) SEM image of partially crushed hollow spheres at high magnification. (e) TEM image of hollow silica spheres at low magnification. (f) High-magnification TEM image of the mesoporous shell.

the Stöber method have a mean diameter of about 550 nm and consist of radially oriented ordered mesostructure (Figure 1b and Figure S1 in the Supporting Information). After being incubated with water at room temperature for 48 h and treated with acidic ethanol to removal CTAB templates, the mesoporous silica products synthesized by the spontaneous transformation method retain the spherical morphology and original size (Figure 1c). The silica spheres crushed by grinding clearly reveal the hollow structure (Figure 1d). Moreover, it is worth noting that the hollow spheres possess a rough interior surface, which is different from the hollow materials prepared by the hard or soft template methods. This is an indication that the hollow structure undergoes an internal transformation process. TEM image (Figure 1e) of the spheres shows a noticeable contrast between the core and the shell, which further confirms the hollow structure. It can also be clearly observed that the spheres have an average diameter of 550 nm and a mean shell thickness of about 110 nm. The particle size as observed from dynamic light scattering (DLS) is 638 nm (Table S1, Supporting Information), that is, the TEM image analysis slightly underestimates the size measured in solution. High-magnification TEM image shows that the mesochannels of the spheres are continuous throughout the shell with openings at surface and are radially oriented to the sphere surface (Figure 1f), which means that the mesochannels of the hollow spheres are readily accessible. It favors the adsorption and release of guest molecules, such as anticancer drugs. It is

dx.doi.org/10.1021/cm303338v | Chem. Mater. 2013, 25, 98−105

worth mentioning that the yield of the hollow spheres is measured to be as high as 81.1% after the transformation, demonstrating the outer layer of the Stöber silica spheres is more compact than the inner part. Therefore, the hollow structure is quite stable. Even after being calcined at 600 °C for 5 h or treated under 40-kHz ultrasound for 10 min, no broken spheres are formed. Besides, the success rate for formation of hollow structure is 100% by the facile process, indicating the spontaneous self-transformation method is highly reproducible. Moreover, grams of products can be easily prepared by a large reaction system (Figure S2, Supporting Information), which provides great potential for their practical applications.

The XRD pattern of the mesoporous silica hollow spheres shows three diffraction peaks, associated with the 100, 110, and 200 reflections of hexagonal symmetry with the space group *p6mm* (Figure 2a). This is in good agreement with that of the

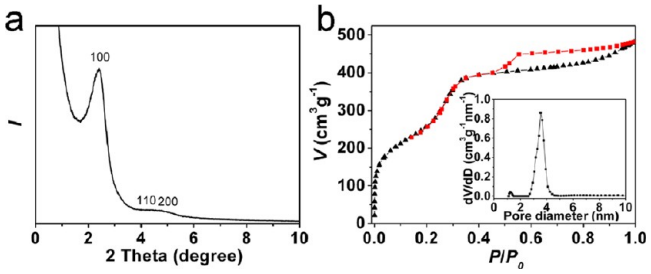

Figure 2. (a) XRD pattern, (b) nitrogen sorption isotherm, and the inset pore size distribution curve of the mesoporous silica hollow spheres prepared via the simple spontaneous self-transformation method.

as-made bulk mesoporous silica MCM-41,[37,38] suggesting a similar ordered hexagonal mesostructure. The d_{10} spacing of the mesostructure is 3.7 nm, which corresponds to a unit cell parameter of 4.3 nm. Nitrogen sorption isotherm of the mesoporous silica hollow spheres shows a type IV curve according to the IUPAC nomenclature with a sharp capillary condensation step and a hysteresis loop in the p/p_0 range 0.4–1.0 (Figure 2b), revealing characteristics of mesoporous materials with narrow pore size distribution. The surface area and pore volume are calculated to be as high as about 920 m^2 g^{-1} and 0.75 cm^3 g^{-1}, respectively. The detailed pore size distribution calculated based on the nonlocal density functional theory reveals the hollow spheres have uniform mesopores and micropores of about 3.5 and 1.2 nm, respectively (inset in Figure 2b). These micropores in the silica framework are very important for facilitating accessibility of water molecules and the transfer of silica species during the hollowing process. The mesopore wall thickness is estimated to be 0.8 nm by calculating the difference between unit cell parameter and the pore size. In comparison, the surface area, pore volume, and pore size of the solid-core structured mesoporous silica spheres prepared in the same Stöber solution without the transformation process are calculated to be about 940 m^2 g^{-1}, 0.47 cm^3 g^{-1}, and 3.0 nm, respectively (Figure S3, Supporting Information). These results indicate that the self-transformation process can also significantly enlarge the pores, which would be much better for loading large biomolecules.

The solid-to-hollow transformation was carefully monitored after incubating the as-made mesostructured silica spheres in water. Figure 3a–c shows a complete cycle of morphology change of silica spheres at room temperature. After aging in water for 2 h, the silica spheres are still solid, and their diameter is almost identical to that of the as-prepared samples (Figure 3a). Interestingly, the spheres show a clear contrast between a dark periphery and a gray central part with prolonged incubation time, indicating that the water molecules diffuse into the interior of silica spheres and lead to a selective etching inside (Figure 3b). Continued reaction further removes materials from particle cores, making the appearance of hollow structures more pronounced (Figure 3c). This is suggestive of a time-dependent transformation process. Compared to the as-prepared samples, the hollow particles retain the spherical morphology, smooth surface, and original diameter after the structure transformation, suggesting that the inner section is preferentially etched in water. When placed in water for much longer period of time, the hollow silica spheres do not exhibit significant changes in shell thickness, suggesting that an equilibrium is reached between the silica particles and solution

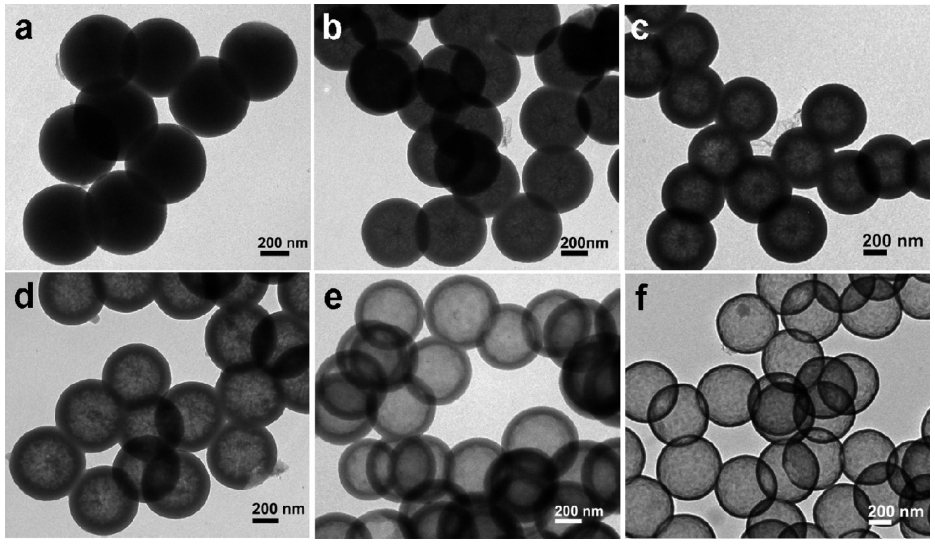

Figure 3. TEM images of the hollow silica spheres prepared by incubating the Stöber method derived silica in water at room temperature for (a) 2, (b) 6, and (c) 48 h; at 70 °C for (d) 2 and (e) 48 h; and (f) at 90 °C for 48 h.

dx.doi.org/10.1021/cm303338v | *Chem. Mater.* 2013, 25, 98–105

at room temperature. The rate of the spontaneous self-transformation and the final shell thickness are found to be dependent on the temperature of water. Increasing the temperature to 70 °C dramatically shortens the solid-to-hollow conversion time to 2 h (Figure 3d). Simultaneously, by incubating the Stöber method derived silica in water for 2−48 h, the shell thickness of the hollow spheres can vary from 95 to 70 nm (Figure 3d and e). The silicon content of the dissolved silica in the water was determined by ICP-AES. The results show that the silicon concentration is significantly increased after incubating the Stöber silica spheres in water for 2 h at 70 °C and then plateaued thereafter (Figure S4, Supporting Information). These results are consistent with the TEM observations that the inner section of the as-made silica spheres is more readily dissolved and the outmost layer is relatively robust in water. Further increasing the temperature of water to 90 °C, hollow silica spheres with a shell thickness of 25 nm were obtained after dispersing the original Stöber silica spheres in water for 48 h (Figure 3f). It is noted that the silica hollow spheres with the thin shell thickness of 25 nm are still stable enough to maintain a spherical shape upon preparation, isolation, and imaging, which can facilitate potential applications as reactors or carries on chemical or biomedical fields.

The diameter of the mesoporous silica hollow spheres can be modulated by controlling the ethanol/water volume ratio of the Stöber solution. While the etching temperature is fixed at 70 °C and time is 12 h, a decrease in particle size is observed when the ethanol/water ratio is decreased from 0.54 to 0.35. Under these reaction conditions, the highest ethanol/water ratio (0.54) results in particles with the largest size and shell thickness, approximately 480 and 53 nm, respectively (Figure 4a). As the ethanol/water ratio decreases to 0.46, 0.40, and 0.35, the average particle sizes change to 430, 340, and 255 nm (Figure 4b−d), respectively. Simultaneously, the shell thickness of the hollow spheres also decreases form 36 to 26 nm. The DLS measurements show that the hydrodynamic sizes of the hollow spheres decrease form 478 to 281 nm when the ethanol/water ratio is decreased from 0.54 to 0.35 (Table S1, Supporting Information), which is consistent with the TEM observations.

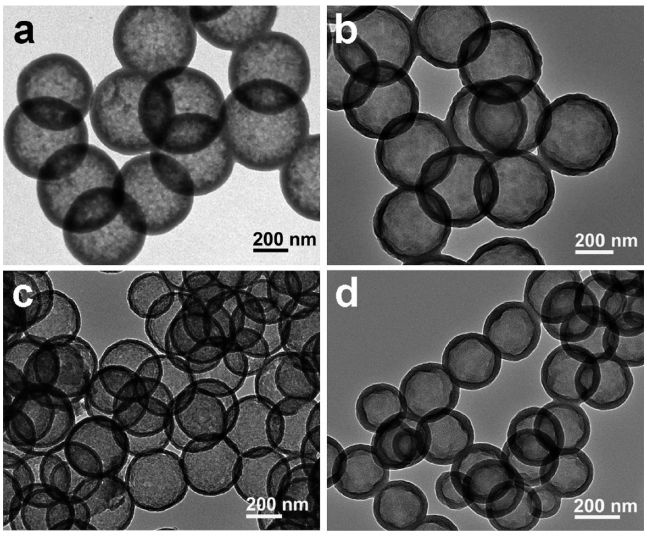

Figure 4. TEM images of the mesoporous silica hollow spheres prepared with ethanol/water volume ratio of (a) 0.54, (b) 0.46, (c) 0.40, and (d) 0.35.

The yields of the hollow spheres with the sizes of 480 nm, 430 nm, 340 nm, and 255 nm are 42.5%, 49.4%, 48.8%, and 50.0%, respectively. The fact that the yields are lower than that of the hollow spheres with the size of 550 nm is attributed to their thin shell thicknesses. The ζ-potential of the mesoporous silica hollow spheres with various sizes is measured to be −25.3 to −34.9 mV (Table S1, Supporting Information), indicating their highly negatively charged surfaces because of the silanol groups present on the particles are known to have a low isoelectric point of around pH 2.[39]

Considering the inner part of silica spheres is less exposed to the water than the outermost layer during the transformation process, the fact that the inner section is preferentially dissolved is very interesting. ^{29}Si MAS NMR spectra of the as-made Stöber silica spheres and the hollow silica prepared by the self-transformation method were recorded to directly analyze the degree of silica condensation (Figure 5). In the spectra, the

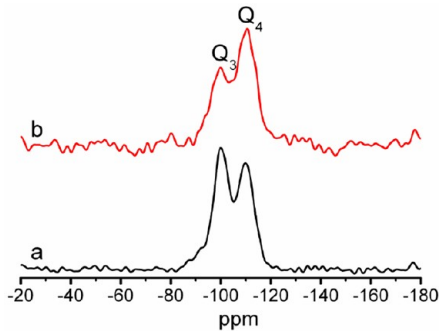

Figure 5. ^{29}Si MAS NMR spectra of (a) as-made Stöber silica spheres and (b) hollow silica spheres prepared by incubating the original sample in water at room temperature for 48 h.

signals at −100 and −110 ppm correspond to the Q_3 [$(SiO)_3SiOH$] and Q_4 [$(SiO)_4Si$] silicate species, respectively. It is obvious that the Q_4/Q_3 ratio of hollow silica is much higher than that of the as-made Stöber silica spheres, suggesting a significantly increased number of silicon atoms fully coordinated to nearest neighbors of other silicates of hollow silica as compared to that of as-made Stöber silica; viz., the degree of condensation of hollow silica spheres is much higher than that of original Stöber silica spheres. We further studied the detailed reactions, under which the original solid Stöber silica spheres are formed, to probe the origin of the inhomogeneity. It was found that reaction temperature of the Stöber solution plays an important role for the formation of hollow structure. When the reaction temperature is increased from 15 to 45 °C, while the etching temperature is fixed at 70 °C and time is 2 h, the shell thickness of hollow spheres increases from 35 to 150 nm (Figure 6a). Further increasing the reaction temperature higher than 45 °C, the final structural is solid after the transformation process. The ethanol/water ratio is another important factor for the formation of hollow structure. Decreasing the ratio leads to an obvious decrease of the shell thickness (Figure 6b). Further decreasing it to lower than 0.46, only solid silica spheres are yielded after transformation at 70 °C for 2 h. In addition, when the TEOS is decreased from 56 mM to 28 mM, the finally obtained silica is also solid in structure.

Based on these results, we speculate that the transformation of Stöber method derived silicate-CTAB composite spheres from solid to hollow structure in water is induced by a low

dx.doi.org/10.1021/cm303338v | Chem. Mater. 2013, 25, 98−105

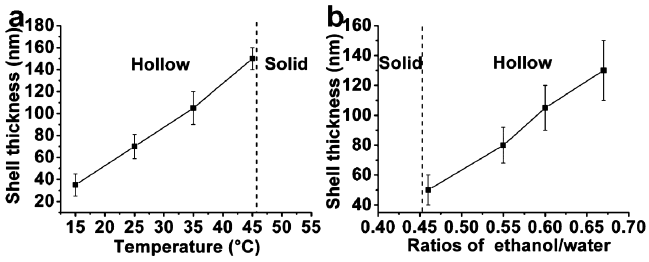

Figure 6. Variation of the shell thickness and structure of the silica products as a function of the (a) temperature and (b) ethanol/water volume ratio of the Stöber solution.

degree of silica condensation in their inner section. When TEOS molecules are added to an ethanol aqueous solution, they are consecutively hydrolyzed to give 1−4 hydroxyl groups and assembled with CTAB surfactants via the electrostatic interaction to form mesostructured silica spheres.[40,41] Due to the slow hydrolysis of TEOS in the Stöber solution at low temperature and high ethanol/water ratios, a gradient of increasing chemical stability forms as the TEOS species assembled with CTAB are increasingly hydrolyzed. As such, the outmost layer is much more compact than the inner section, as it is mostly derived from the condensation of silicic acid and its aggregates. In comparison, inner parts are less dense, which are a result from a lower degree of cross-linking due to the presence of more Si-OC_2H_5 groups in the areas. Simultaneously, these Si-OC_2H_5 groups in the framework can induce more ethanol included in the inner section. The less compact inner silicate-CTAB composites are more easily attacked by water and redissolved, and migrate outward until an equilibrium is reached.[33,42] When the Stöber method derived mesostructured spheres are mixed with water, the water molecules rapidly diffuse into the interior of the silicate-CTAB composite framework via the micropores in the spheres. The inner section of composite spheres is etched, and the solid silica particles are eventually transformed into hollow structured spheres upon continued etching. The dissolved silica species in water may be redeposited on the mesostructured silica shells during the aging process. The dissolution of silica species can be accelerated with the increases of temperature due to increased solubility and dissolution rate, and thus, the hollowing process is shortened.

The spontaneous self-transformation also provides a facile way for fabricating yolk−shell structures with functional interior core, hollow space, and permeable mesoporous outer shell. It is well-known that numerous inorganic materials including metals and metal oxides can be coated by silica to form core−shell structured composites. We further demonstrate that the silica coated composites can be used to create yolk−shell structures via a surfactant-assembly sol−gel coating process and a following spontaneous self-transformation procedure. For example, uniform core−shell Fe_3O_4@nSiO_2 spheres with a magnetite core and a nonporous silica layer were first prepared according to our previously reported method[34−36] (Figure S5, Supporting Information). Then, a mesostructured CTAB/SiO_2 composite was deposited on the Fe_3O_4@nSiO_2 spheres in a Stöber solution by using CTAB as a structure-directing agent and TEOS as a silica source, resulting in Fe_3O_4@nSiO_2@CTAB/SiO_2 microspheres (Figure 7a). After incubating with water at 70 °C for 1 h, the CTAB/SiO_2 composite was gradually etched as evidenced by the reduced contrast at the inner section (Figure 7b). Finally, the original solid structure

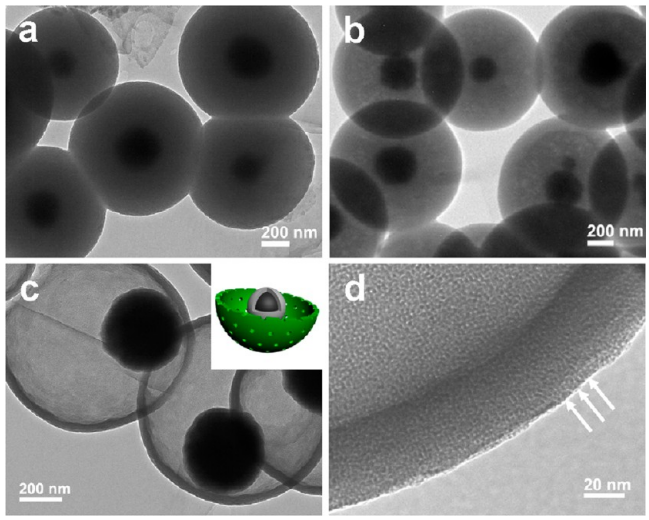

Figure 7. TEM images showing the structure evolution of Fe_3O_4@nSiO_2@CTAB/SiO_2 microspheres: (a) the original samples; (b−c) the samples after incubating with water for (b) 1 and (c) 12 h; (d) TEM image of the mesoporous shell. Inset in (c) is the structure model of the yolk−shell microspheres.

transforms to yolk−shell structure with Fe_3O_4@nSiO_2 inside silica shell after 12 h of incubation (Figure 7c). High-magnification TEM image shows the shell of the yolk−shell microspheres also possesses radially oriented mesochannels with openings at both surfaces (Figure 7d). The inclusion of Fe_3O_4@nSiO_2 cores endows the yolk−shell microspheres with a saturation magnetization as high as 38 emu g^{-1} and allows the convenient separation and recycling by applying external magnetic fields (Figure S6, Supporting Information). Also, the T_2* enhancing capability of the magnetic yolk−shell spheres was investigated by using a clinical 3 T magnetic resonance imaging (MRI) scanner. The signal intensity of MRI decreases with the increase of the concentration of the yolk−shell spheres (Figure S7, Supporting Information). The r_2* relaxivity of the yolk−shell spheres is measured to be as high as 441 mM^{-1} s^{-1}, demonstrating the potential application in T_2*-weighted magnetic resonance imaging. Besides, the large cavities between the magnetic core and mesoporous shell could store large quantities of guest molecules, while the mesoporous shell with radially oriented mesochannels provides large accessible pores for the adsorption and encapsulation of biomacromolecules. Moreover, the designed yolk−shell spheres possess uniform size and good structural stability. All these properties make the composite materials ideal candidates for biomedical applications such as MRI, targeted drug delivery, or bioseparation.

The applications of the mesoporous silica hollow spheres in biomedicine fields must guarantee the biocompatibility of the materials. The biocompatibility of mesoporous silica nanospheres (MSNs) has been widely studied in recent works.[43,44] In contrast, only a few works have investigated the biocompatibility of the mesoporous silica hollow spheres.[6] In fact, although the framework is the same, the mesoporous silica hollow spheres have more advantages than the MSNs in biomedical applications. First, the hollow spheres can load much more cargos than the MSNs owing to their large void space. Second, the weight of the hollow spheres will be less than that of the MSNs if the same number of particles is injected into the body, which means that less silica will interact

dx.doi.org/10.1021/cm303338v | *Chem. Mater.* 2013, 25, 98−105

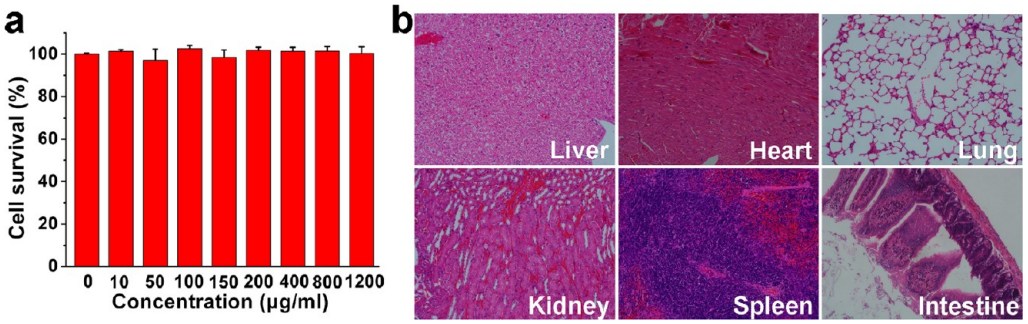

Figure 8. (a) In vitro viability of human embryo kidney 293T cells incubated with mesoporous silica hollow spheres at different concentrations. (b) Representative tissue sections of mice stained with hematoxylin and eosin. All images shown here are 200× magnification.

with the biological systems. So, the in vitro and in vivo biocompatibility assessments of the mesoporous silica hollow spheres are necessary. The effects of the mesoporous silica hollow spheres on cell proliferation were assessed with human embryo kidney 293T cells by CCK-8 assay (Figure 8a). The viability of untreated cells was assumed to be 100%. Notably, the cell viability retained about 100%, even when they were incubated with the hollow spheres at a concentration of as high as 1.2 mg mL^{-1} for 24 h. Histological assessment was further used to investigate the toxicity of the mesoporous silica hollow spheres. Analysis was performed on the tissues obtained from the harvested organs (liver, heart, lung, kidney, spleen, and intestine). As shown in Figure 8b, hepatocytes in the liver samples appear normal, and there are no inflammatory infiltrates and steatosis. Cardiac muscle tissue in the heart samples shows no hydropic degeneration. No pulmonary fibrosis and inflammation are observed in the lung samples. No apparent tissue injury, inflammation, lesions, or necrosis is observed in the other organs. These results clearly indicate that the mesoporous silica hollow spheres possess an excellent biocompatibility, indicating they have promising potentials for applications in biomedicine fields.

As proof-of-concept for their application in biomedicine, the mesoporous silica hollow spheres were filled with perfluorocarbon gas to prepare an ultrasound contrast agent. The less water-soluble perfluorocarbon gas could go inside the silica spheres through the mesoporous shells and stay in the hollow interiors to form gas bubbles for contrast enhanced imaging. The ultrasound imaging of the gas-filled silica spheres in PBS with different concentrations was investigated in conventional B mode and harmonic mode. As shown in Figure 9, the ultrasound signals gradually increase with the increase of silica sphere concentrations in the both modes. Clearly, ultrasound imaging can be obtained as the concentration of hollow spheres is above 2 mg mL^{-1}. In contrast, there are no signals observed in the conventional B mode when solid-core structured mesoporous silica spheres are used as a control (Figure S8, Supporting Information). Simultaneously, the signals of the solid particles observed under the harmonic mode are also obviously lower than that of the hollow spheres. Such in vitro results demonstrate that the mesoporous silica hollow spheres have the potential for ultrasound imaging applications.

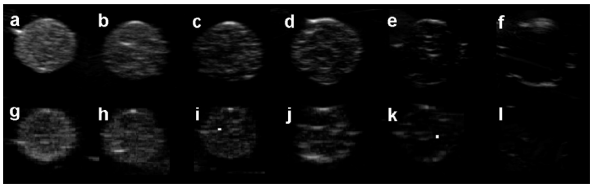

Figure 9. In vitro ultrasound imaging of the mesoporous silica hollow spheres under (a–f) conventional B mode and (g–l) harmonic mode with concentrations of (a,g) 16, (b,h) 8, (c,i) 4, (d,j) 2, (e,k) 1, and (f,l) 0 mg mL^{-1}, respectively, in PBS.

4. CONCLUSIONS

Uniform mesoporous silica hollow spheres with ordered and radially oriented mesopore channels have been successfully prepared via the spontaneous self-transformation approach by dispersing the Stöber method derived silica spheres in water. The self-transformation method is intrinsically simple and does not require any sacrificial templates, emulsion droplets, surface protective agents, or corrosive and toxic etching agents. The formation of mesoporous silica hollow spheres undergoes a gradually etching process in the inner section, while outmost silica layer keeps intact. The obtained mechanically stable hollow spheres possess tunable diameter, smooth surface, and a uniform shell thickness. The mesochannels of the hollow spheres are highly oriented, open, and accessible. The NMR characterization and detailed reactions demonstrate that low condensation degree of inner section of the Stöber silica spheres is a determining factor for the formation of hollow structure. The excellent biocompatibility of the hollow spheres was demonstrated by its negligible cytotoxicity against human embryo kidney 293T cells and no obvious histological lesion in major organs. Besides, the potential application of mesoporous silica hollow spheres as contrast agents for ultrasound imaging was also demonstrated in vitro. Moreover, on the basis of the spontaneous self-transformation strategy, yolk–shell structures with functional interior core, hollow space, and mesoporous outer shell can be realized, providing many new exciting opportunities in fabrication of multifunctional materials for various applications.

■ ASSOCIATED CONTENT

Supporting Information

TEM image of the mesostructured Stöber silica sphere. Table of particle sizes measured by TEM and DLS as well as ζ-potentials of mesoporous silica hollow spheres prepared with different ethanol/water volume ratios. Photo of the mesoporous silica hollow spheres prepared by a 10× reaction system. Nitrogen sorption isotherm and pore size distribution curve of the solid-core structured mesoporous silica spheres prepared in the Stöber solution. Variation of the concentration of the dissolved silicon species in water as a function of time at 70 °C. TEM images of Fe_3O_4 particles and Fe_3O_4@nSiO_2 spheres.

dx.doi.org/10.1021/cm303338v | *Chem. Mater.* 2013, 25, 98–105

Room-temperature magnetization curves of magnetite particles, Fe_3O_4@nSiO_2 spheres, and yolk−shell structured magnetic microspheres. Relaxation rate R_2* of magnetic yolk−shell microspheres. In vitro ultrasound imaging of solid-core structured mesoporous silica particles. This information is available free of charge via the Internet at http://pubs.acs.org/.

AUTHOR INFORMATION

Corresponding Author

*Fax: +86 25 8480 4659. Tel: +86 25 8086 0185. E-mail: cjr.luguangming@vip.163.com.

Notes

The authors declare no competing financial interest.

ACKNOWLEDGMENTS

We greatly appreciate financial support from the National Natural Science Foundation of China (30930028 and 81201175), the National Key Basic Research Program of the PRC (2011CB707700), and the Major International (Regional) Joint Research Program of China (81120108013). Z.T. acknowledges support from the National Science Foundation for Postdoctoral Scientists of China (2012M521934). We especially appreciate Prof. Gengfeng Zheng of Fudan University and Prof. Xiaoyuan Chen and Dr. Xinglu Huang of National Institutes of Health (NIH) for their comments and suggestions in the preparation of the manuscript. We thank Wei Luo of Fudan University for measuring the nitrogen sorption isotherms.

REFERENCES

(1) Schacht, S.; Huo, Q.; Voigt-Martin, I. G.; Stucky, G. D.; Schüth, F. *Science* **1996**, *273*, 768−771.

(2) Wang, J.; Xiao, Q.; Zhou, H.; Sun, P.; Yuan, Z.; Li, B.; Ding, D.; Shi, A.-C.; Chen, T. *Adv. Mater.* **2006**, *18*, 3284−3288.

(3) Tanev, P. T.; Pinnavaia, T. J. *Science* **1996**, *271*, 1267−1269.

(4) Fang, X.; Liu, Z.; Hsieh, M.-F.; Chen, M.; Liu, P.; Chen, C.; Zheng, N. *ACS Nano* **2012**, *6*, 4434−4444.

(5) Wang, S.; Zhang, M.; Zhang, W. *ACS Catal.* **2011**, *1*, 207−211.

(6) Chen, Y.; Chen, H.; Guo, L.; He, Q.; Chen, F.; Zhou, J.; Feng, J.; Shi, J. *ACS Nano* **2010**, *4*, 529−539.

(7) Du, L.; Liao, S.; Khatib, H. A.; Stoddart, J. F.; Zink, J. I. *J. Am. Chem. Soc.* **2009**, *131*, 15136−15142.

(8) Zhu, Y.; Meng, W.; Gao, H.; Hanagata, N. *J. Phys. Chem. C* **2011**, *115*, 13630−13636.

(9) Tang, F.; Li, L.; Chen, D. *Adv. Mater.* **2012**, *24*, 1504−1534.

(10) Chen, Y.; Chen, H.; Sun, Y.; Zheng, Y.; Zeng, D.; Li, F.; Zhang, S.; Wang, X.; Zhang, K.; Ma, M.; He, Q.; Zhang, L.; Shi, J. *Angew. Chem.* **2011**, *123*, 12713−12717.

(11) Peng, Y.-K.; Lai, C.-W.; Liu, C.-L.; Chen, H.-C.; Hsiao, Y.-H.; Liu, W.-L.; Tang, K.-C.; Chi, Y.; Hsiao, J.-K.; Lim, K.-E.; Liao, H.-E.; Shyue, J.-J.; Chou, P.-T. *ACS Nano* **2011**, *5*, 4177−4187.

(12) Zhang, K.; Chen, H.; Zheng, Y.; Chen, Y.; Ma, M.; Wang, X.; Wang, L.; Zeng, D.; Shi, J. *J. Mater. Chem.* **2012**, *22*, 12553−12561.

(13) Zhao, Y.; Zhang, J.; Li, W.; Zhang, C.; Han, B. *Chem. Commun.* **2009**, 2365−2367.

(14) Li, J.; Liu, J.; Wang, D.; Guo, R.; Li, X.; Qi, W. *Langmuir* **2010**, *26*, 12267−12272.

(15) Wang, J.; Xia, Y.; Wang, W.; Poliakoff, M.; Mokaya, R. *J. Mater. Chem.* **2006**, *16*, 1751−1756.

(16) Liu, J.; Hartono, S. B.; Jin, Y. G.; Li, Z.; Lu, G. Q.; Qiao, S. Z. *J. Mater. Chem.* **2010**, *20*, 4595−4601.

(17) Djojoputro, H.; Zhou, X. F.; Qiao, S. Z.; Wang, L. Z.; Yu, C. Z.; Lu, G. Q. *J. Am. Chem. Soc.* **2006**, *128*, 6320−6321.

(18) Yamada, Y.; Mizutani, M.; Nakamura, T.; Yano, K. *Chem. Mater.* **2010**, *22*, 1695−1703.

(19) Tan, B.; Rankin, S. E. *Langmuir* **2005**, *21*, 8180−8187.

(20) Chen, M.; Wu, L. M.; Zhou, S. X.; You, B. *Adv. Mater.* **2006**, *18*, 801−806.

(21) Chen, Z.; Cui, Z.-M.; Niu, F.; Jiang, L.; Song, W.-G. *Chem. Commun.* **2010**, *46*, 6524−6526.

(22) Zhao, Y.; Lin, L.-N.; Lu, Y.; Chen, S.-F.; Dong, L.; Yu, S.-H. *Adv. Mater.* **2010**, *22*, 5255−5259.

(23) Fang, X.; Chen, C.; Liu, Z.; Liu, P.; Zheng, N. *Nanoscale* **2011**, *3*, 1632−1639.

(24) Stöber, W.; Fink, A.; Bohn, E. *J. Colloid Interface Sci.* **1968**, *26*, 62−69.

(25) Zhang, Q.; Zhang, T.; Ge, J.; Yin, Y. *Nano Lett.* **2008**, *8*, 2867−2871.

(26) Ren, N.; Wang, B.; Yang, Y.-H.; Zhang, Y.-H.; Yang, W.-L.; Yue, Y.-H.; Gao, Z.; Tang, Y. *Chem. Mater.* **2005**, *17*, 2582−2587.

(27) Zhang, L.; Wang, T.; Yang, L.; Liu, C.; Wang, C.; Liu, H.; Wang, Y. A.; Su, Z. *Chem.—Eur. J.* **2012**, *18*, 12512−12521.

(28) Roca, M.; Haes, A. J. *J. Am. Chem. Soc.* **2008**, *130*, 14273−14279.

(29) Chen, D.; Li, L.; Tang, F.; Qi, S. *Adv. Mater.* **2009**, *21*, 3804−3807.

(30) Wong, Y. J.; Zhu, L.; Teo, W. S.; Tan, Y. W.; Yang, Y.; Wang, C.; Chen, H. *J. Am. Chem. Soc.* **2011**, *133*, 11422−11425.

(31) Zhang, T.; Ge, J.; Hu, Y.; Zhang, Q.; Aloni, S.; Yin, Y. *Angew. Chem., Int. Ed.* **2008**, *47*, 5806−5811.

(32) Yu, Q.; Wang, P.; Hu, S.; Hui, J.; Zhuang, J.; Wang, X. *Langmuir* **2011**, *27*, 7185−7191.

(33) Teng, Z.; Zheng, G.; Dou, Y.; Li, W.; Mou, C.-Y.; Zhang, X.; Asiri, A. M.; Zhao, D. *Angew. Chem., Int. Ed.* **2012**, *51*, 2173−2177.

(34) Liu, J.; Sun, Z.; Deng, Y.; Zou, Y.; Li, C.; Guo, X.; Xiong, L.; Gao, Y.; Li, F.; Zhao, D. *Angew. Chem., Int. Ed.* **2009**, *48*, 5875−5879.

(35) Teng, Z.; Zhu, X.; Zheng, G.; Zhang, F.; Deng, Y.; Xiu, L.; Li, W.; Yang, Q.; Zhao, D. *J. Mater. Chem.* **2012**, *22*, 17677−17684.

(36) Teng, Z.; Su, X.; Chen, G.; Tian, C.; Li, H.; Ai, L.; Lu, G. *Colloids Surf., A* **2012**, *402*, 60−65.

(37) Kresge, C. T.; Leonowicz, M. E.; Roth, W. J.; Vartuli, J. C.; Beck, J. S. *Nature* **1992**, *359*, 710−712.

(38) Beck, J. S.; Vartuli, J. C.; Roth, W. J.; Leonowicz, M. E.; Kresge, C. T.; Schmitt, K. D.; Chu, C. T.-W.; Olson, D. H.; Sheppard, E. W.; McCullen, S. B.; Higgins, J. B.; Schlenker, J. L. *J. Am. Chem. Soc.* **1992**, *114*, 10834−10843.

(39) Iler, P. K. *The Chemistry Of Silica*; Wiley-Interscience: New York, 1979.

(40) Van Blaaderen, A.; Van Geest, J.; Vrij, A. *J. Colloid Interface Sci.* **1992**, *154*, 481−501.

(41) Wei, J.; Yue, Q.; Sun, Z. K.; Deng, Y. H.; Zhao, D. Y. *Angew. Chem., Int. Ed.* **2012**, *51*, 6149−6153.

(42) Alexander, G. B.; Heston, W. M.; Iler, R. K. *J. Phys. Chem.* **1954**, *58*, 453−455.

(43) Lu, J.; Liong, M.; Li, Z.; Zink, J. I.; Tamanoi, F. *Small* **2010**, *6*, 1794−1805.

(44) Yu, T.; Malugin, A.; Ghandehari, H. *ACS Nano* **2011**, *5*, 5717−5728.